SCIENTIFIC REPORTS

OPEN

SUBJECT AREAS:
BATTERIES
SYNTHESIS OF GRAPHENE

Received
6 August 2013

Accepted
4 November 2013

Published
19 November 2013

Correspondence and requests for materials should be addressed to H.-T.J. (heetae@kaist.ac.kr)

High quality reduced graphene oxide through repairing with multi-layered graphene ball nanostructures

Kyoung Hwan Kim[1], MinHo Yang[2], Kyeong Min Cho[1], Young-Si Jun[3], Sang Bok Lee[2,4] & Hee-Tae Jung[1]

[1]Department of Chemical and Biomolecular Engineering, Korea Advance Institute of Science and Technology (KAIST), Daejeon 305-701 (Korea), [2]Graduate School of Nanoscience and Technology (WCU), Korea Advanced Institute of Science and Technology (KAIST), Daejeon 305-701 (Korea), [3]Material Department and Department of Chemistry & Biochemistry, University of California, Santa Barbara, CA 93106 (United States), [4]Department of Chemistry and Biochemistry, University of Maryland, College Park, MD 20742 (United States).

We present a simple and up-scalable method to produce highly repaired graphene oxide with a large surface area, by introducing spherical multi-layered graphene balls with empty interiors. These graphene balls are prepared via chemical vapor deposition (CVD) of Ni particles on the surface of the graphene oxides (GO). Transmission electron microscopy and Raman spectroscopy results reveal that defects in the GO surfaces are well repaired during the CVD process, with the help of nickel nanoparticles attached to the functional groups of the GO surface, further resulting in a high electrical conductivity of 18,620 S/m. In addition, the graphene balls on the GO surface effectively prevent restacking of the GO layers, thus providing a large surface area of 527 m^2/g. Two electrode supercapacitor cells using this highly conductive graphene material demonstrate ideal electrical double layer capacitive behavior, due to the effective use of the outstanding electric conductivity and the large surface area.

Synthesis of highly repaired graphene oxides which have high electrical conductivity and large surface area is one of the most important issues in graphene research, as most large scale graphene-based applications use a suspension of graphene oxide (GO) or reduced graphene oxide (rGO) due to its large scale production at low cost. Unfortunately, the oxidation process generally introduces significant defects in the as-synthesized graphene oxide, degrading its unique properties such as superior carrier mobility, mechanical strength and chemical stability[1,2].

Several different methods, which include chemical reduction[3–5], thermal assisted reduction[6–11], metal doping[12], organic compounds hybridization[13], and hydrocarbon gas assisted chemical vapor deposition[14–16], have been primarily used to restore the original characteristics of graphene. Chemical reducing agents, such as hydrazine[3,4] and alcohol[5], were used to repair graphene oxide by removing hydroxyl and epoxide groups on the graphene sheets. In addition, thermal treatment using various heating sources such as a furnace[6–9], microwave[10], and laser[11] could reduce graphene oxide by eliminating oxygen functionalities through the release of gaseous molecules of H_2O, CO, and CO_2 at high temperature. In spite of the intensive research efforts in this field, many limitations in the production of high quality graphene from the chemically driven graphene remain, because oxygen functionalities cannot be perfectly removed, and defects (e.g. missing carbon atoms, holes on the carbon network) are not sufficiently repaired by these approaches[17]. Furthermore, it is very difficult to control the reduction level using a chemical reduction process. As for the thermal treatments, rapid expansion of graphene oxide during heating also produces a considerable number of defects in the graphene lattice, although thermally reduced GO (TRGO) shows relatively good restoration of electrical conductivity at high temperature. These defects can vitiate the electrical and mechanical qualities of graphene.

Moreover, reduced GO (rGO) is prone to re-stacking due to strong π-π interactions and van der Waals forces between the planar basal planes of graphene sheets. It is therefore very difficult to obtain highly conductive graphene with a large surface area from graphene oxide. Although other methods such as metal doping[12], organic compounds hybridization[13], and hydrocarbon gas assisted chemical vapor deposition[14–16] have been suggested to enhance the electrical properties of graphene oxides, they are largely limited to a thin film type process, which is not adaptable for mass production. Hence, a simple method for large-scale production of highly repaired conductive graphene oxide without restacking is extremely desirable in the field of graphene research.

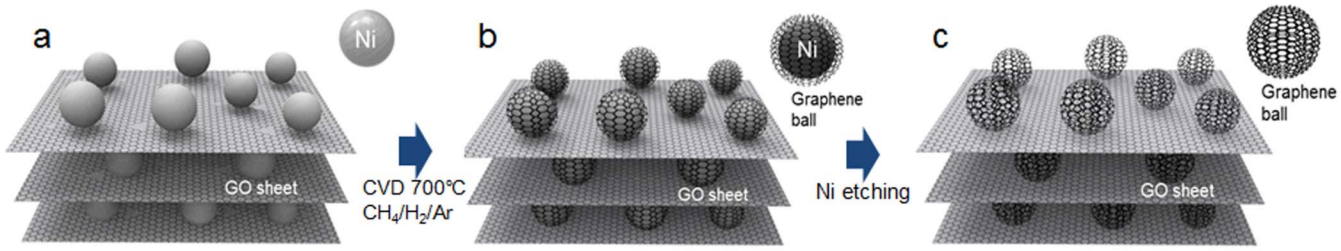

Figure 1 | (a–c) Schematic illustration of the synthesis of repaired graphene oxide sheets/multi-layered graphene balls 3D hybrids (RGGB).

Here, we report a new method for fabricating highly repaired graphene oxide with a large surface area, by incorporating multi-layered graphene balls onto graphene oxide sheets. In this synthesis, nickel nanoparticles, attached to the oxygen functionalities of the graphene oxide surface, serve not only as a template for the CVD grown multi-layered graphene balls, but also as a catalyst for the repairing of defects in the graphene oxide sheets. It is found that defects of the GO surfaces are highly repaired during the CVD process, with the help of the attached nickel nanoparticles, resulting in a high electrical conductivity of 18,620 S/m. Moreover, the graphene balls prevent the agglomeration of graphene sheets, thus ensuring a large specific surface area (~527 m^2/g). This highly repaired graphene oxide with graphene balls (RGGB) shows good electric double layer capacitor (EDLC) performance, arising from the superior electrical conductivity and large surface area.

Results

The overall synthesis process is depicted in Figure 1. The graphene oxide-nickel nanoparticle composite (GONi) was first prepared by mixing the GO dispersion in water with the 0.1 M $NiCl_2$ solution in ethanol, followed by addition of a reduction agent, hydrazine. Abundant oxygen functionalities (e.g. carboxyl, hydroxyl, and epoxide) on the GO surface act as reactive sites for the nucleation and growth of nickel nanoparticles[18]. The hydrazine not only reduces the GO, but also yields nickel hydrazine complexes such as $Ni(N_2H_4)_2Cl_2$ *or* $Ni(N_2H_4)_3Cl_2$ on the surface of the GO[19]. When NaOH is put into the mixed solution, nickel hydroxide (NiOH) is formed by ligand exchange of the Cl_2 ion with OH^-. Further reaction with hydrazine produces the GO-Ni composite: $[2Ni^{2+} + N_2H_4 + 4OH^- \rightarrow 2Ni + N_2 + 4H_2O]$ (Fig. 1 a). Next, the spherical multi-layered graphenes, named graphene balls, were prepared on the surface of the nickel particles by chemical vapor deposition (CVD) at 700°C with CH_4 gas. The carbon dissolution and precipitation steps produce multi-layered graphenes on the nickel surface[20,21]. (Fig. 1 b) It is crucial to note that copper is not suitable for producing the graphene ball, because mainly single layer graphene is produced on the copper surface[22,23], and the single layer graphene balls are easily collapsed after removing the copper core. Thus, nickel was used to grow multi-layered graphene on the GO surface, and the repaired graphene oxide with multi-layered graphene balls (RGGB) was successfully produced after removing the nickel cores by hydrochloric acid solution. (Fig. 1 c)

Wide-angle x-ray scattering (WAXS) was performed in order to monitor the changes in structure of GONi after the CVD process at different temperatures. As-synthesized GONi exhibits prominent diffraction peaks of nickel (JCPDS #.04-0850), which indicates that the nickel particles were formed on the graphene sheets (Fig. 2, black line). In addition, no clear graphite (002) peak ($2\theta \sim 26.5°$) that can be attributed to the diffraction of multi-layered graphene balls was observed in the as-prepared GO-Ni composites, because the nickel nanoparticles hinder the restacking of graphene layers. The graphite peak becomes noticeable from a temperature of 700°C (Fig. 2, green

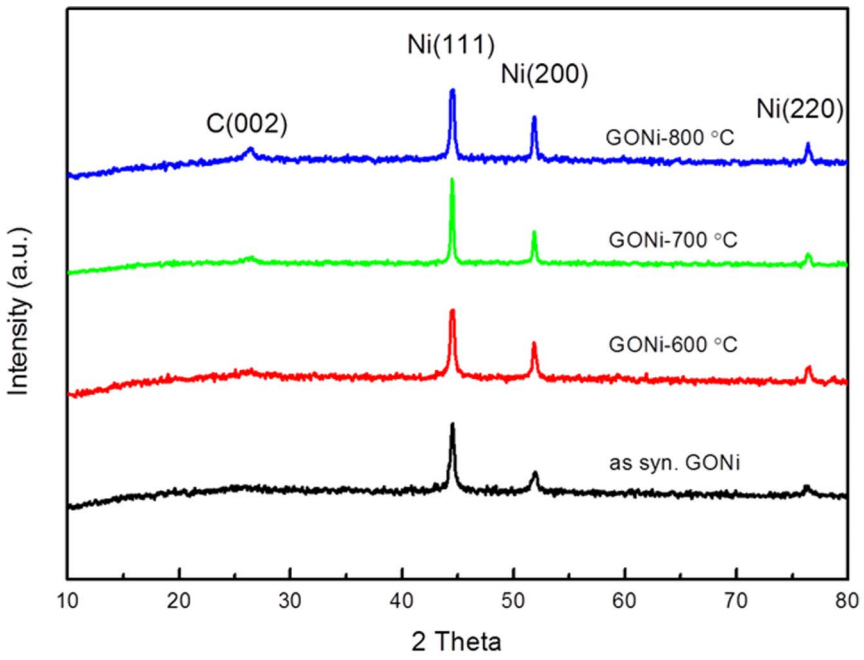

Figure 2 | **WAXS patterns of GONi after the CVD process at different temperatures; (black) As-synthesized, (red) 600°C, (green) 700°C, and (blue) 800°C.**

line), indicating the presence of multi-layered graphene balls on the nickel surface. The peak becomes more prominent at 800°C, with increasing graphene layers of the balls (Fig. 2, blue line). It must be noted though, that we cannot exclude the possibility of the restacking of graphene oxide during the CVD process at high temperature, due to the sintering of intercalated nickel nanoparticles. In fact, nickel nanoparticles are easily sintered and agglomerated at high temperature, and it is thus hard to maintain the shape and size of the initial Ni nanoparticles[24]. Accordingly, we selected 700°C as the CVD temperature. The size of the nickel nanoparticles on the synthesized GONi is sub 100 nm (Fig. S1 a), and this is maintained until 700°C with thin graphene ball layers (Fig. S1 c). On the other hand, the Ni particles severely sintered at 800°C, resulting in an increase in the size of the nickel particles and the thickening of the layers of the graphene balls (Fig. S1 d). Hence, the highly conductive repaired graphene oxide with multi-layered graphene balls (RGGB) was prepared at 700°C, and the nickel core was removed by hydrochloric acid. The energy dispersive X-ray spectroscopy (EDX, Fig. S2), and the wide-angle x-ray scattering (WAXS, Fig. S3) measurements confirmed that the nickel particles surrounded by graphene balls were successfully removed after hydrochloric acid treatment.

Figure 3 shows scanning electron microscopy (SEM) and transmission electron microscopy (TEM) images of the well dispersed multi-layered graphene balls on the repaired graphene oxide sheet. Figure 3a shows these well dispersed multi-layered graphene balls formed on the graphene sheets. Most of the graphene balls are spherical, but ellipsoidal balls also coexist[25]. Due to the short CVD reaction time (10 min), the carbon layer is likely to sustain the ellipsoidal shape. In addition, most of the graphene balls are under 100 nm in diameter, indicating that sintering of nickel nanoparticles is not severe at 700°C. Graphene balls under 100 nm in size are well dispersed on the graphene sheets (Fig. 3b), and the inset high-resolution TEM image shows a multi-layered graphene ball (~10 layers). This image also indicates that the multi-layered graphene grows on the nickel surface without the growth of amorphous carbon. Figure 3c shows a repaired graphene sheet with a graphene ball, in which the basal plane of the repaired graphene sheet exhibits a hexagonal electron diffraction (ED) pattern (Figure 3d). This clearly indicates that the graphene oxide is greatly reduced and repaired, and each graphene sheet is not restacked. In general, the ED pattern of representative GO exhibits a broad ring shape pattern due to the many defects and holes produced during the severe oxidation process (Fig. S4)[26,27]. The hexagonal array of 2D carbon atoms thus shows that the graphene balls have been successfully formed on the graphene oxide sheets, which have been effectively repaired through the optimized CVD process.

To further verify the successful repair of the graphene sheets by the graphene balls, Raman spectroscopy was performed at 633 nm laser, comparing the RGGB with chemically (N_2H_4) reduced GO (HRGO) and thermally (700°C) reduced GO (TRGO) (Figure 4 a,b). Two prominent peaks at ~1355 cm^{-1}(D) and 1575 cm^{-1}(G), and two smaller peaks at ~1600 cm^{-1}(D′) and ~2700 cm^{-1}(2D) are attributed to graphitic carbon materials[28–30]. RGGB has two types of Raman spectra as shown in Figure 4a. The first spectrum (black line) comes from the repaired graphene oxide sheets, and has a relatively high D peak. The other spectrum (red line) originates from the multi-layered graphene balls, and is similar to the typical spectrum of carbon nanotubes (CNT) grown on transition metal surfaces[31,32]. The 2D peak position of the graphene ball is slightly upshifted with respect to repaired graphene oxide sheets because of its multiple layers, and is similar to the Raman spectrum of common multi-layered graphene sheets (<10 layers)[28]. Figure 4b shows a comparison of the Raman spectrum of the graphene sheet of RGGB with those of HRGO and TRGO. The ratio of the D peak to the G peak intensity, I_D/I_G, for the graphene sheet of RGGB (I_D/I_G = 0.91) has the lowest value, compared to that of HRGO (I_D/I_G = 1.32) and

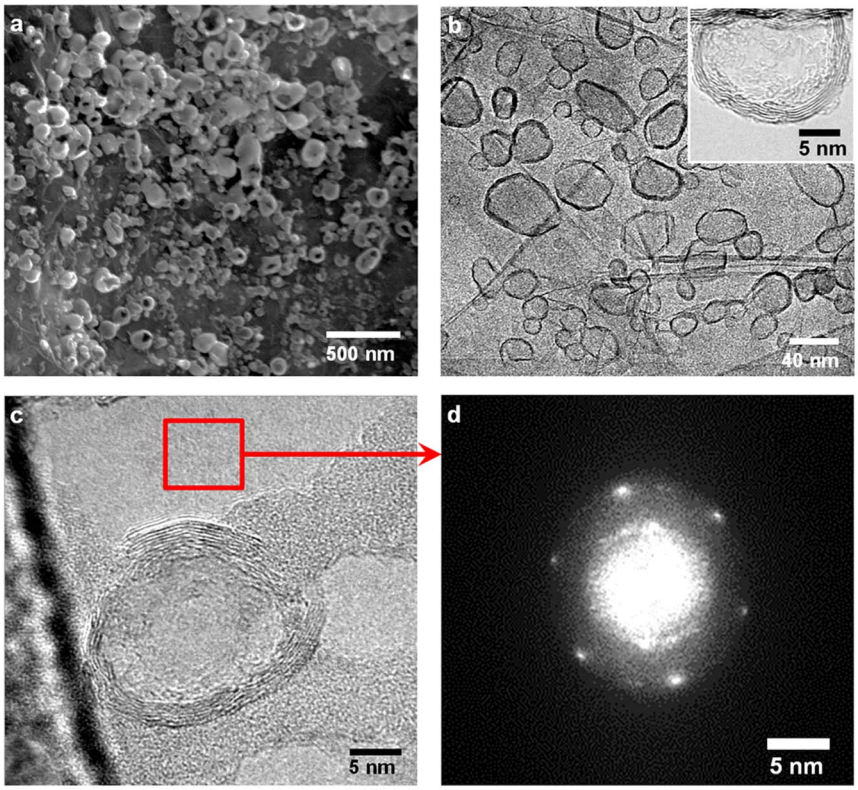

Figure 3 | (a, b) SEM and TEM images of RGGB that display well dispersed multi-layered graphene balls on graphene sheets. (inset) High-resolution TEM image of a multi-layered graphene ball. (c) High-resolution TEM image of RGGB. (d) Selected area electron diffraction pattern (SAED) of the basal plane of the repaired graphene oxide sheets.

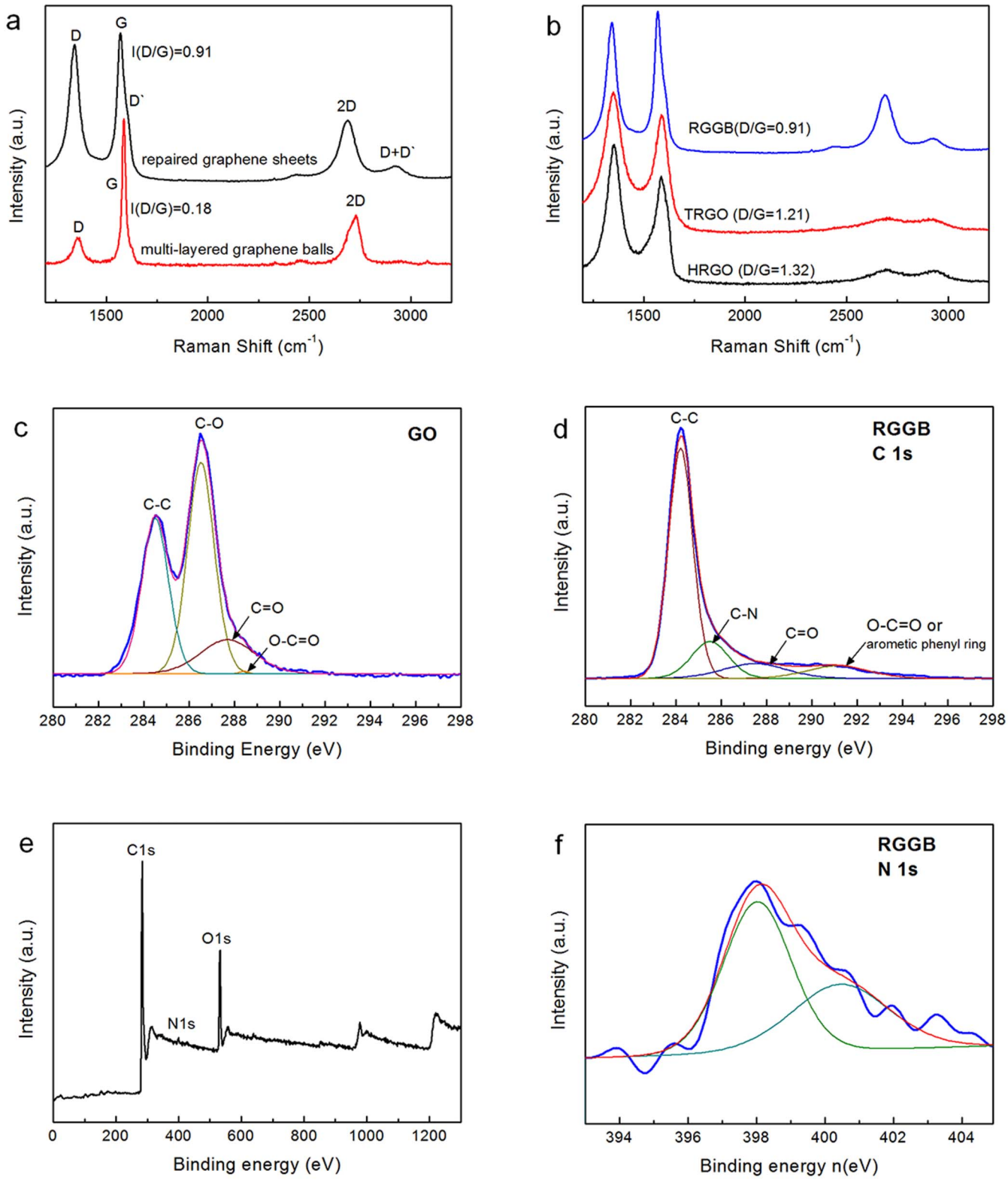

Figure 4 | (a) Two types of Raman spectra of RGGB. (b) Raman spectrum of different reduction treatments (RGGB, TRGO, HRGO) using a 633 nm laser. The C1s XPS spectra of (c) as-synthesized GO and (d) RGGB. (e) The survey XPS spectra of RGGB, and (f) N1S XPS spectra of RGGB.

TRGO (I_D/I_G = 1.21)[15]. This result indicates the effective removal of defects and the restoration of sp2 carbon during the Ni assisted CVD process, as the ratio of D/G is directly related to the average size of the sp2 carbon domain[33]. In addition, the 2D peak of the graphene sheet of RGGB is sharp with a high intensity, and the peak position is below that of the graphene ball. This implies that the repaired graphene sheets have maintained their single layer without restacking during the CVD process at 700°C, as the 2D peak is generally upshifted with increasing layers of graphene sheets[28].

To analyze the change in the oxidation functionalities of carbon during the process, X-ray photoelectron spectroscopy (XPS) was used (Figure 4 c–f). The XPS spectrum of GO shows three prominent

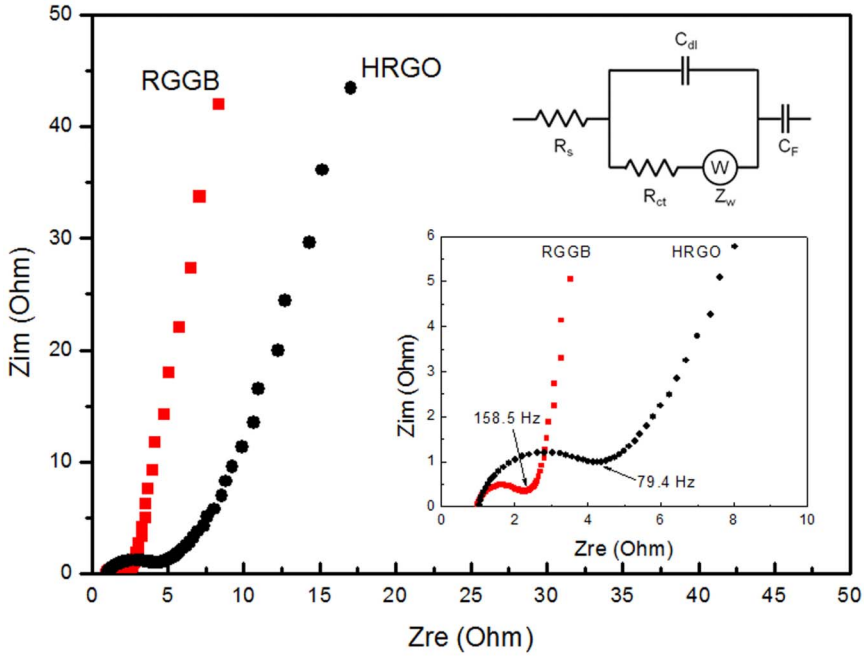

Figure 5 | Nyquist plots for RGGB and HRGO electrodes measured with AC amplitude of 10 mV over the frequency range of 100 kHz and 0.01 Hz. (The inset shows the magnified high frequency regions.).

peaks at 284.3 eV, 286.5 eV, and 287.5 eV, corresponding to -C-C- bonds, -C-O- bonds, and –C=O bonds respectively (Fig. 4c)[2,34,35]. In comparison, the intensities of the -C-O- and -C=O functional groups were significantly reduced in RGGB (Fig. 4d). The main peak at 284.3 eV indicates the graphite-like sp2 -C-C- bond, thereby showing that most of the carbon atoms are arranged in a honeycomb lattice. A new peak at 285.5 eV corresponds to C-N bonds[2]. The C/O atomic ratios were significantly increased from 1.67 (HRGO) to 5.67 (RGGB), indicating that most of the oxygen functional groups were successfully reduced. Interestingly, nitrogen was observed in Figure 4e. The high resolution N 1s spectrum of RGGB (Fig. 4f) shows two peaks at 397.9 eV and 399.6 eV, corresponding to C=N and C≡N respectively[36]. Recent results have demonstrated that the oxygen containing functionalities present on GO, such as carbonyl and carboxylic groups, cause C-N bond formation during reduction with hydrazine[2]. N doping can modify graphene electronic properties because it contributes to additional charge carriers.

To further support the reduction in the number of oxygen functional groups, Fourier Transform-Infrared spectroscopy (FT-IR) was used (Fig. S5), by comparing RGGB with GO and HRGO. The FT-IR spectrum indicates that the O-H stretching vibration at 3400 cm^{-1} for GO was eliminated in both the spectra of HRGO and RGGB, but the C=O double bond at 1724 cm^{-1} and C-O stretching vibrations at 1200 cm^{-1} still remain on the HRGO. However, RGGB has few functional groups, and has almost the same FT-IR spectra as pristine graphite, indicating that most of the carboxyl, hydroxyl, and epoxide groups have been reduced by CVD process.

Electrical conductivities of RGGB samples were determined using a pellet-type sample with a four–point probe[37]. The thickness of each sample was estimated by optical microscope and scanning electron microscopy (SEM) (Fig. S6). RGGB is highly electrically conductive at **18,620 S/m** (t = 183 μm). (Table S1) HRGO was used as a reference sample under identical conditions, showing an electrical conductivity of 1,589 S/m (t = 162 μm). It is noteworthy that the pellet-type RGGB sample shows comparable electrical conductivity with thin film type reduced graphene samples[38]. Compared to HRGO, RGGB thus shows more than 10 times the electrical conductivity, indicating that the GO sheet of GONi was successfully repaired during the CVD process at 700°C, with the help of the nickel catalyst. This is in agreement with the hexagonal pattern in the SAED of the repaired graphene sheet. In our approach, Ni particles are likely to be attached to the oxygen functional groups on the GO sheets[18]. The repair of defects in graphene can only occur on the top-most layer[19], thus it is important to have nickel on the defects sites of each individual graphene sheet. Owing to the catalytic effect of Ni during the CVD process, defects on the graphene sheets are repaired to produce a hexagonal array of carbon atoms, resulting in superior electrical conductivity. When we consider that the electrical conductivity of a common graphene-based carbon electrode is under 1,200 S/m (Table S2), the high conductivity of the RGGB is very significant.

Based on the N_2 adsorption analysis, a specific surface area of 527 m^2/g was determined for RGGB, which is 53% higher than for HRGO (340 m^2/g)[39]. (Fig. S7) This is a direct result of the graphene balls successfully preventing the restacking of graphene sheets and providing additional surface area. When we consider general GO easily restacks in ambient conditions because of the π-π interaction between graphene sheets, the presence of graphene balls on graphene sheets becomes very important. RGGB can thus maintain its high surface area under the storage in air condition due to the graphene balls.

Discussion

To show the novelty of the high electrical conductivity and porous network of RGGB, an impedance test was conducted over a frequency range of 100 kHz to 0.01 Hz. Using the circuit depicted in Figure 5, the Nyquist plot for RGGB shows a sharp increment in the imaginary part of the impedance, demonstrating an ideal capacitive behavior. (Fig. 5)[40–42] Compared to the plot of HRGO, it has an almost vertical line plot in the low frequency region. (Fig. 5, inset) The charge transfer resistance (Rct) of RGGB is 0.91 ohm, which is much lower than that of HRGO (Rct = 3.73 ohm). Moreover, the knee frequency of RGGB is 158.5 Hz, indicating better ion diffusion ability than HRGO (79.4 Hz) because the porous network of RGGB provides sufficient void space. In the high frequency region, RGGB shows a smaller semicircle plot, which means that it has lower resistivity than HRGO. This result is in agreement with the superior electrical conductivity of RGGB (~**18,620 S/m**) as compared to HRGO (~1,589 S/m).

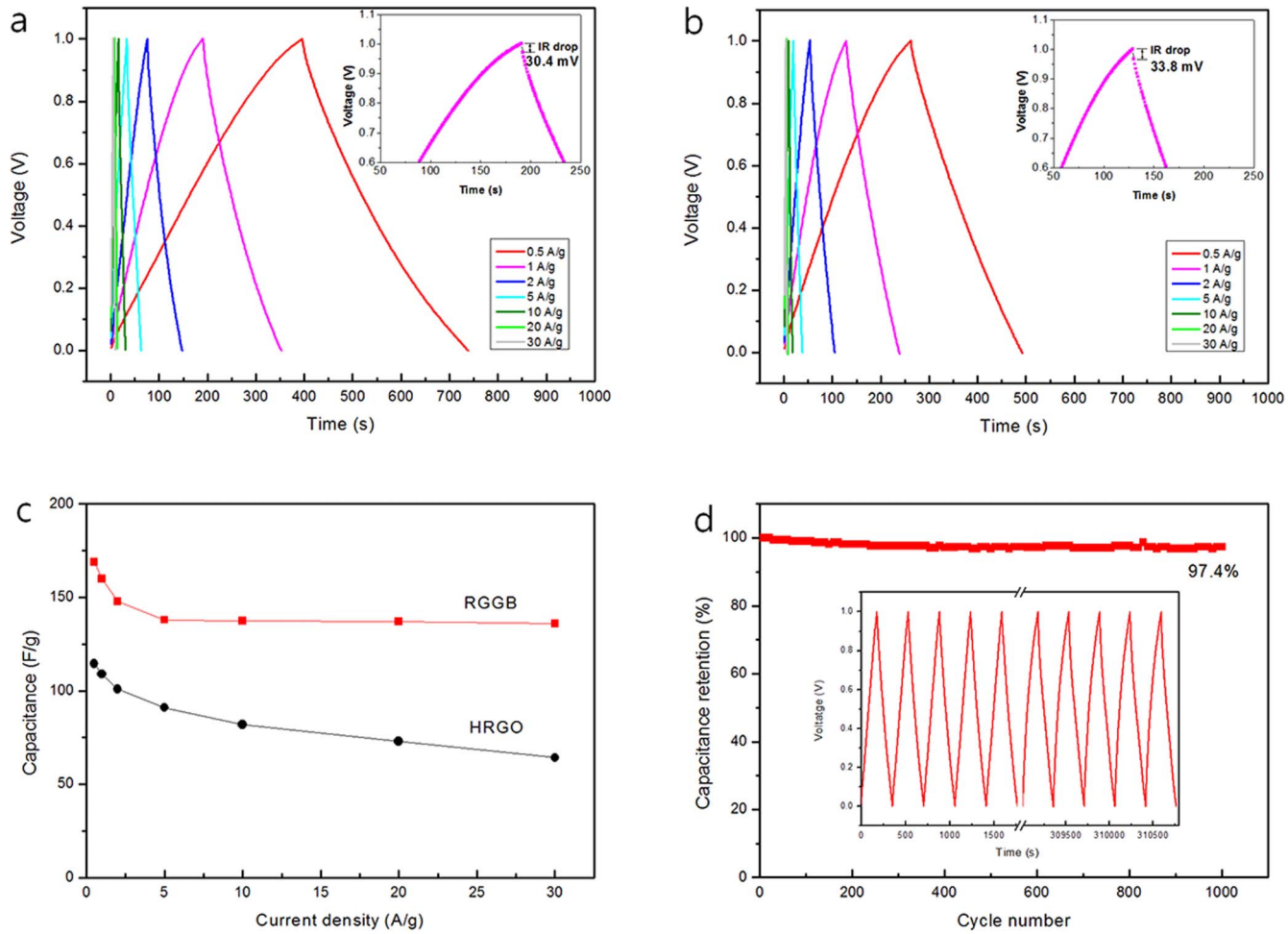

Figure 6 | Galvanostatic charge/discharge curves of (a) RGGB, and (b) HRGO under different current densities of 0.5, 1, 2, 5, 10, 20, and 30 A/g, with the IR drops against the current density of 1 A/g in the inset. (c) Dependencies of the specific capacitance of RGGB and HRGO electrodes on various current densities, ranging from 0.5 to 30 A/g, for charge/discharge behavior. (d) Cycling stability of RGGB measured with a two-electrode cell at a constant current density of 1 A/g over 1000 cycles.

This fabrication approach has the additional advantages of adaptability to mass production (Fig. S8), and nickel recyclability. During the nickel removing process, the reaction of nickel and hydrochloric acid produces hydrogen gas and nickel chloride [$Ni + 2HCl \rightarrow NiCl_2 + H_2$], permitting the recovery and re-use of $NiCl_2$. Figure S9 shows $NiCl_2$ solution before and after use, and both solutions possess the same yellowish-green color, indicating the presence of $NiCl_4^{2-}$ in aqueous solution[43]. This shows that it is possible to recycle the nickel precursors. Because the disposal of heavy metals can cause severe environmental problems, recyclability of nickel is a significant factor from an industrial point of view.

To evaluate the electrochemical performance of RGGB with high electrical conductivity and a large surface area, we measured the performance of supercapacitor cells using two electrode systems with 1 M H_2SO_4 electrolyte. For reference samples, HRGO was tested under identical conditions. In Figure S10, the RGGB electrode shows nearly symmetrical rectangular shapes for the cyclic voltammetry (CV) curves with various scan rates in the range of 0.0 to 1.0 V, indicating an ideal electrical double layer capacitive behavior[40]. The capacitive performance was further investigated from the galvanostatic charge/discharge profile in Figures 6 a and b. The curves at various current densities (0.5–30 A/g) exhibit a nearly triangular shape, suggesting that both fast electron transfer and ion diffusion occurred in the RGGB electrode. Based on the discharge curve line, the specific capacitance of the RGGB was **171 F/g** at 1 A/g, which is 50% higher than for HRGO (114 F/g at 1 A/g). Compared to other graphene-based supercapacitors listed in Table S2, our supercapacitor devices show good specific capacitance without an additional pseudo-capacitance[44,45], due to effective use of the large specific surface area and high electric conductivity. The insets of Figures 6a and b show the IR drop at the discharge current density of 1 A/g, which indicates the internal resistance of the cells. Because a portion of the total internal resistance is attributed to the choice of electrode material[46], RGGB with a higher conductivity shows an IR drop 10% lower than that of HRGO. The results correspond to the Nyquist plots, and suggest the high rate capability of the RGGB electrode.

Figure 6c shows the capacitance retention of RGGB at different charge/discharge current densities. At high current density, RGGB still displays a high specific capacitance value (**80%** capacitance retention at 30 Ag^{-1}) as compared to HRGO (56% capacitance retention at 30 Ag^{-1}), again indicating that the higher electrical conductivity of RGGB facilitates charge-transfer, and that the larger space provided by the multi-layered graphene balls allows for effective ion diffusion even at high charging/discharging rates. In addition, the cycling stability, which is the one of the most critical requirements for practical application, was tested with a two-electrode cell at a constant current density of 1 A/g. The RGGB electrode retained **97.4%** of its initial specific capacitance even after 1000 cycles, indicating the good electrochemical stability of RGGB. (Fig. 6d)

In summary, we have developed a simple and up-scalable method to produce highly conductive repaired graphene oxide, by adding multi-layered graphene balls onto the GO surface. With the help of a nickel catalyst, defects in the graphene oxide sheet are successfully repaired, and multi-layered graphene balls are simultaneously formed on the nickel nanoparticles by the CVD process. After removing nickel with hydrochloric acid, the resulting RGGB has a superior electrical conductivity of **18,620 S/m** and a large specific surface area of 527 m^2/g. Moreover, the recyclability of the nickel catalyst makes the process more attractive to industry as an environmentally friendly method. The resulting repaired graphene oxide shows ideal electrical double layer capacitive behavior, due to effective use of the high electrical conductivity coupled with the large specific surface area. The RGGB's superior properties, such as high electrical conductivity, large surface area, and chemical stability, make it attractive for various potential electrochemical applications, including energy storage (lithium ion battery, lithium-air battery, or lithium-sulfur battery), sensors, photo-catalysts, and environmental protection.

Methods

Preparation of GO. Graphene oxide was first synthesized using a modified Hummers method. Graphite powder (1 g, Aldrich) was first added to sulfuric acid (98%, 30 ml). Then, potassium permanganate (3.5 g), an oxidizing agent, was gradually added to the graphite solution with vigorous stirring for 10 min. After allowing the reaction to proceed at 35°C for 2 h, the solution was cooled in an ice bath and diluted with deionized water (200 ml). In the following 1 h of stirring, hydrogen peroxide (100 ml) was added to the reaction solution. The mixture was then filtered and washed several times with hydrochloric acid (10%). The remaining solvent was evaporated under vacuum at room temperature for 12 h. As prepared GO are comprised of isolated single to few layer sheets with 1 nm of height and 1 ~ 5 μm of flake size, with the typical Raman spectrum of GO (Figure S11)[1].

Synthesis of repaired graphene/multi-layered graphene ball composite (RGGB). GO was suspended in deionized water and ultrasonically treated for 1 h. The GO dispersion was mixed with nickel chloride (0.1 M in ethanol, Aldrich), and the mixture was vigorously stirred at 70°C for 2 h, followed by addition of hydrazine monohydrate (35 wt% in H_2O, Aldrich). After reaction at 70°C for 2 h, the magnetic stirring bar was removed and the solution was shaken for 2 h with 1 M NaOH solution. The resulting solution was filtered and washed with EtOH and H_2O in order to remove the remaining sodium and chloride salts. The powder was then heated to 700°C using a tube furnace with argon gas, followed by the insertion of CH_4 and H_2 gas for 10 min. Finally, the repaired graphene/multi-layered graphene balls composite (RGGB) was obtained by dissolving the nickel using hydrochloric acid solution.

Material characterizations. The prepared samples were characterized by X-ray diffraction (XRD, Rigaku D/Max-RB (12 KW)) using Cu Kα radiation (λ = 0.15406 nm), scanning electron microscopy (SEM, FEI Nova230), a transmission electron microscope (TEM, Philips Technai F20), an atomic force microscope (AFM, Park systems XE-100), Raman spectroscopy (Horiba Jobin Yvon ARAMIS) using Ar ion CW Laser (514.5 nm), X-Ray photoelectron spectroscopy (XPS, Thermo VG Scientific Sigma Probe), and Fourier-transform infrared spectroscopy (FT-IR, Bruker Alpha-P). N_2 adsorption was carried out at 77 K by a Micromeritics ASAP 2000. The electrical conductivity of the samples was measured using the four-point probe technique (Loresta-GP, Mitsubihi Chemical) with a pellet sample (13 mm in diameter) pressurized at 0.6 ton for 30 s at room temperature.

Electrochemical characterization. Electrochemical measurements were carried out using two-electrode sandwich-type construction cells with a separator (nitrocellulose film) between the two symmetrical working electrodes. The electrolyte used was 1 M H_2SO_4 solution, and a stainless steel (SS) foil was used as a current collector. A mixture containing 95 wt% active material and 5 wt% poly(vinylidene fluoride) binder in N-methyl-2-pyrrolidone was well mixed and then pressed onto the SS foil (1.0×10^7 Pa). The electrochemical performance of the prepared electrodes was characterized by cyclic voltammetry (CV), electrochemical impedance spectroscopy (EIS) measurements, and galvanostatic charge-discharge tests. The experiments were performed using a VersaSTAT 3 (Princeton Applied Research) workstation controlled by a computer.

1. Zhu, Y. *et al.* Graphene and Graphene Oxide: Synthesis, Properties, and Applications. *Adv. Mater.* **22**, 3906–3924 (2010).
2. Stankovich, S. *et al.* Synthesis of graphene-based nanosheets via chemical reduction of exfoliated graphite oxide. *Carbon* **45**, 1558–1565 (2007).
3. Chen, H., Muller, M. B., Gilmore, K. J., Wallace, G. G. & Li, D. Mechanically Strong, Electrically Conductive, and Biocompatible Graphene Paper. *Adv. Mater.* **20**, 3557–3561 (2008).
4. Youn, S. C. *et al.* Effect of the exposure time of hydrazine vapor on the reduction of graphene oxide films. *J. Nanosci. Nanotechnol.* **11**, 5959–5964 (2011).
5. Dreye, D. R., Murali, S., Zhu, Y., Ruoff, R. S. & Bielawski, C. W. Reduction of graphite oxide using alcohols. *J. Mater. Chem.* **21**, 3443–3447 (2011).
6. Yang, D. *et al.* Chemical analysis of graphene oxide films after heat and chemical treatments by X-ray photoelectron and Micro-Raman spectroscopy. *Carbon* **47**, 145–152 (2009).
7. Schniepp, H. C. *et al.* Functionalized Single Graphene Sheets Derived from Splitting Graphite Oxide. *J. Phys. Chem. B* **110**, 8535–8539 (2006).
8. Mattevi, C. *et al.* Evolution of Electrical, Chemical, and Structural Properties of Transparent and Conducting Chemically Derived Graphene Thin Films. *Adv. Funct. Mater.* **19**, 2577–2583 (2009).
9. Geng, J. *et al.* A Simple Approach for Preparing Transparent Conductive Graphene Filmes Using the Controlled Chemical Reduction of Exfoliated Graphene Oxide in an Aqueous Suspension. *J. Phys. Chem. C* **114**, 14433–14440 (2010).
10. Zhu, Y. W. *et al.* Microwave assisted exfoliation and reduction of graphite oxide for ultracapacitors. *Carbon* **48**, 2118–2122 (2010).
11. Sokolov, D. A., Shepperd, K. R. & Orlando, T. M. Formation of Graphene Features from Direct Laser-Induced Reduction of Graphite Oxide. *J. Phys. Chem. Lett.* **1**, 2633–2636 (2010).
12. Kong, B.-S., Geng, J. & Jung, H.-T. Layer-by-Layer Assembly of Graphene and Gold Nanoparticles by Vacuum Filtration and Spontaneous Reduction of Gold Ions. *Chem. Commun.* **16**, 2174–2176 (2009).
13. Geng, J. & Jung, H.-T. Porphyrin Functionalized Graphene Sheets in Aqueous Suspensions: From the Preparation of Graphene Sheets to Highly Conductive Graphene Film. *J. Phys. Chem. C.* **114**, 8227–8234 (2010).
14. Lopez, V. *et al.* Chemical Vapor Deposition Repair of Graphene oxide: A Route to Highly Conductive Graphene Monolayers. *Adv. Mater.* **21**, 4683–4686 (2009).
15. Kholmanov, I. N. *et al.* Healing of Structural Defects in the Topmost Layer of Graphite by Chemical Vapor Deposition. *Adv. Mater.* **23**, 1675–1678 (2011).
16. Cheng, M. *et al.* Restoration of graphene from graphene oxide by defect repair. *Carbon* **50**, 2581–2587 (2010).
17. Mao, S., Pu, H. & Chen, J. Graphene oxide and its reduction: modeling and experimental progress. *RSC Adv.* **2**, 2643–2662 (2012).
18. Goncalves, G. *et al.* Surface modification of graphene nanosheets with gold nanoparticles: The role of oxygen moieties at graphene surface on gold nucleation and growth. *Chem. Mater.* **21**, 4796–4802 (2009).
19. Park, J. W. *et al.* Preparation of fine Ni powders from nickel hydrazine complex. *Mater. Chem. Phys.* **97**, 371–378 (2006).
20. Reina, A. *et al.* Large Area, Few-Layer Graphene Films on Arbitrary Substrates by Chemical Vapor Deposition. *Nano Lett.* **9**, 30–35 (2009).
21. Zhang, Y. *et al.* Comparison of Graphene Growth on Single-Crystalline and Polycrystalline Ni by Chemical Vapor Deposition. *J Phys. Chem. Lett.* **1**, 3101–3107 (2010).
22. Li, X. *et al.* Large-Area Synthesis of High-Quality and Uniform Graphene Films on Copper Foils. *Science* **324**, 1312–1314 (2009).
23. Kim, D. W., Kim, Y. H., Jeong, H. S. & Jung, H.-T. Direct visualization of large-area graphene domains and boundaries by optical birefringency. *Nature Nanotech.* **7**, 29–34 (2012).
24. Cao, L. F. *et al.* Thermal stability of Fe, Co, Ni metal nanoparticles. *Phys. Stat. Sol. (b)* **243**, 2745–2755 (2006).
25. Helveg, S. *et al.* Atomic-scale imaging of carbon nanofibre growth. *Nature* **427**, 426–429 (2004).
26. Stankovich, S. *et al.* Graphene-based composite materials. *Nature* **442**, 282–286 (2006).
27. Zhang, J. *et al.* Reduction of graphene oxide via L-ascorbic acid. *Chem. Commun.* **46**, 1112–1114 (2010).
28. Ferrari, A. C. Raman spectroscopy of graphene and graphite: Disorder, electron-phonon coupling, doping and nonadiabatic effects. *Solid State Commun.* **143**, 47–57 (2007).
29. Kudin, K. *et al.* Raman Spectra of Graphite Oxide and Functionalized Graphene Sheets. *Nano Lett.* **8**, 36–41 (2008).
30. Eckmann, A. *et al.* Probing the Nature of Defects in Graphene by Raman Spectroscopy. *Nano Lett.* **12**, 3925–3930 (2012).
31. Boskovic, B. O., Stolojan, V., Khan, R. U. A., Haq, S. & Silva, S. R. P. Large-area synthesis of carbon nanofibres at room temperature. *Nature Mater.* **1**, 165–168 (2002).
32. Jorio, A. *et al.* Characterizing carbon nanotube samples with resonance Raman scattering. *New J. Phys.* **5**, 139.1–139.17 (2003).
33. Tuinstra, F. & Koenig, J. L. Raman spectrum of graphite. *J. Chem. Phys.* **53**, 1126–1130 (1970).
34. Tien, H. N. *et al.* Enhanced solvothermal reduction of graphene oxide in a mixed solution of sulfuric acid and organic solvent. *Chem. Eng. J.* **211–212**, 97–103 (2012).
35. Bagri, A. *et al.* Structural evolution during the reduction of chemically derived graphene oxide. *Nature Chem.* **2**, 581–587 (2010).

36. Ech-chamikh, E., Essafti, A., Ijdiyaou, Y. & Azizan, M. XPS study of amorphous carbon nitride (a-C:N) thin films deposited by reactive RF sputtering. *Sol. Energy Mater. Sol. Cells* **90**, 1420–1423 (2006).
37. Choi, B. G., Yang, M., Hong, W. H., Choi, J. W. & Huh, Y. S. 3D Macroporous Graphene Frameworks for Supercapacitors with High Energy and Power Densities. *ACS Nano* **6**, 4020–4028 (2012).
38. Han, J. *et al.* Solution-based production of graphene nano-platelets containing extremely low amounts of heteroatoms. *Solid state Sci.* **25**, 1–5 (2013).
39. Wang, Y. *et al.* Supercapacitor Devices Based on Graphene Materials. *J Phys. Chem. C* **113**, 13103–13107 (2009).
40. Taberna, P. L., Simon, P. & Fauvarque, J. F. Electrochemical Characteristics and Impedance Spectroscopy Studies of Carbon-Carbon Supercapacitors. *J. Electrochem. Soc.* **150**, A292–A300 (2003).
41. Zhang, L. & Shi, G. Preparation of Highly Conductive Graphene Hydrogels for Fabricating Supercapacitors with High Rate Capability. *J. Phys. Chem. C* **115**, 17206–17212 (2011).
42. Zhang, L. L. *et al.* Highly Conductive and Porous Activated Reduced Graphene Oxide Films for High-Power Supercapacitors. *Nano Lett.* **12**, 1806–1812 (2012).
43. Gill, N. S. *et al.* Tetrahalo Complexes of Dipositive Metals in the First Transition Series. *Inorg. Synth.* **9**, 136–142 (1967).
44. Raymundo-Piñero, E., Cadek, M. & Beguin, F. Tuning carbon materials for supercapacitors by direct pyrolysis of seaweeds. *Adv. Funct. Mat.* **19**, 1032–1039 (2009).
45. Hsieh, C. T. & Teng, H. Influence of oxygen treatment on electric double-layer capacitance of activated carbon fabrics. *Carbon* **40**, 667–674 (2002).
46. Stoller, M. D. & Ruoff, R. S. Best practice methods for determining an electrode material's performance for ultracapacitors. *Energy Environ. Sci.* **3**, 1294–1301 (2010).

Acknowledgments

This work was supported by the Global Frontier Research Center for Advanced Soft Electronics (no. 2011-0032062, MSIP), and the National Research Foundation of Korea (NRF) grant funded by the Korean government (no. 2012R1A2A1A01003537, MSIP). SBL were supported (electrochemical characterization) as part of the Nanostructures for Electrical Energy Storage (NEES), an Energy Frontier Research Center funded by the US Department of Energy, Office of Science, Office of Basic Energy Sciences under Award Number DESC0001160.

Author contributions

K.H.K. and H.-T.J. wrote the manuscript. K.H.K. and K.M.C. prepared the samples and performed characterization. M.Y. and S.B.L. involved the electrochemical analysis. Y.-S.J. guided the Nickel nanoparticle synthesis and helped with data analysis. H.-T.J. supervised the work.

Additional information

Supplementary information accompanies this paper at http://www.nature.com/scientificreports

Competing financial interests: The authors declare no competing financial interests.

How to cite this article: Kim, K.H. *et al.* High quality reduced graphene oxide through repairing with multi-layered graphene ball nanostructures. *Sci. Rep.* **3**, 3251; DOI:10.1038/srep03251 (2013).